Eur. Phys. J. AP **5**, 237–242 (1999)

THE EUROPEAN PHYSICAL JOURNAL APPLIED PHYSICS

Determination of the electron mean free path in the 1–1.8 eV energy range in thin gold layers using ballistic electron emission microscopy

R. Coratger[a], C. Girardin, R. Pechou, F. Ajustron, and J. Beauvillain

CEMES/CNRS, 29 rue J. Marvig, B.P. 4347, 31055 Toulouse Cedex 4, France

Received: 21 September 1998 / Revised and accepted: 15 December 1998

Abstract. Electron mean free path (λ_a) has been investigated using Ballistic Electron Emission Microscopy (BEEM). Using the average collector current computed from large scale BEEM images and a model in which the current exponentially decreases in terms of metal thickness, a constant value of $\lambda_a = 11$ nm has been calculated in the 1–1.8 eV electron energy range. On small scale images, the study of well-defined BEEM domains shows that either λ_a or the interface transmission factor (or both) may differ from their average values. These local variations from one grain to another are interpreted as interface defects and channeling of the electron beam due to the electronic and crystallographic of the gold layer.

PACS. 61.16.-d Electron, ion, and scanning probe microscopy – 73.40.Ns Metal-nonmetal contacts

1 Introduction

Since its invention by Kaiser and Bell in 1988 [1], Ballistic Electron Emission Microscopy (BEEM) has proven to be an adequate technique for the study of buried Metal-Semiconductor interfaces. The operating principle of this microscopy can be formulated as follows: electrons ballistically injected by the tip of a Scanning Tunneling Microscope in a thin metal layer may overcome the potential barrier between the metal and the semiconductor on which it is deposited provided electrons exhibit adequate kinetic energy. Measurement of the energy threshold allows the Schottky barrier height to be determined with a large energetic and spatial resolution. Therefore, most BEEM applications deal with Schottky barrier height determination and interface structures. After the pioneering work of Kaiser and Bell on Au/Si(100) and Au/GaAs(100) [2], BEEM experiments have been performed on contacts involving III-V semiconductors such as GaP [3] or on Metal/II-VI junctions [4–6]. Other experiments have also been carried out on specific semiconductor heterostructures [7–9].

However, this technique can also be used to study other mechanisms such as carrier diffusion in the metal overlayer or at the interface. Intensity of the current collected in the semiconductor strongly depends on transport properties in the metal layer as well as on quantum transmission at the interface. The collector current intensity vanishes as the metal thickness increases compared to the electron attenuation length in the metal (typically about 10 nm for 1 eV electrons). This parameter is of fundamental importance and may be studied using either ballistic electron emission spectroscopy or BEEM imaging.

In this paper, electron attenuation length, λ_a, in thin gold layers has been investigated using BEEM imaging for electron energies from 1 to 1.8 eV. This has shown that λ_a is independent of the electron energy in this energy window and that domains of different behaviours may be evidenced on non-epitaxial gold layers.

2 Experimental

A home-built pocket-size Scanning Tunneling Microscope (STM) working in air has been slightly modified to allow controlled voltage variations between tip and sample during an experiment and simultaneous acquisition of the collector current variations with a picoampere resolution (see Fig. 1). For ballistic electron emission spectroscopy (BEES), the collector current (I_{BEEM}) variations are recorded as a function of bias voltage. For BEEM imaging, the metal surface is raster-scanned at a constant tunneling current (from 1 to 20 nA) and the I_{BEEM} variations are simultaneously recorded. For this, the bias voltage used must be higher than the Schottky barrier height at the metal-semiconductor interface. Thus two images are obtained: the STM topography of the metal surface and the local variations of I_{BEEM} shown in grey levels. Each data file is stored in a computer for subsequent data processing.

Samples consist of n type Si(100) (P doping at 10^{19} cm^{-3}) substrates covered by an 11 μm Si epitaxial layer, P doped at 10^{15} cm^{-3}. The silicon sample is cleaned in an (HF:methanol, 1:4) solution and a 150 nm

[a] e-mail: coratger@cemes.fr

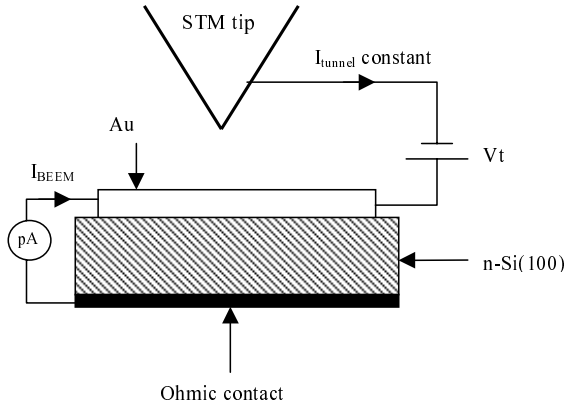

Fig. 1. Schematic diagram of the experimental setup.

thick gold layer is thermally evaporated on the back of the Si wafer. An ohmic contact is obtained by heating at 300 °C for 5 minutes to allow interface diffusion between Au and Si atoms. The doped Si surface is chemically cleaned and a thin gold layer is thermally deposited on the front side of the sample under Ultra High Vacuum conditions (10^{-8} torr). To reduce leakage currents and noise, evaporation is achieved through use of a mask with 0.5 mm-diameter holes. Gold thickness is given by a quartz crystal microbalance whose accuracy (±10%) had previously been controlled by AFM and STM measurements. Thicknesses of 7.5, 9.5, 12, 14, 16.5, 18.8 and 24.5 nm were selected. As the film is polycrystalline, a smaller thickness may yield non continuous layers. On the other hand, values in excess of 25 nm result in very small currents and low signal-to-noise ratios. The mean roughness of the different gold surfaces turns out to be unchanged (typically 3–4 nm).

Finally, a 50 μm-diameter copper wire is bonded to the gold layer to provide bias voltage while a third electrode is bonded to the ohmic contact. The quality of these junctions is checked using macroscopic $I(V)$ spectra whose ideality factors n are generally in the 1–1.1 range. All Pt–Ir tips are obtained by cutting a 0.25 mm-diameter Pt–Ir wire.

3 Model

To review the different results, a straightforward model has been used in which, the BEEM current is expressed as:

$$I_{\mathrm{BEEM}} = K I_{\mathrm{tunnel}} \mathrm{e}^{-d/\lambda_{\mathrm{a}}}. \quad (1)$$

Its magnitude depends of three factors: the total number of injected carriers given by I_{tunnel}, the exponential attenuation factor which is a function of the metal thickness d and electron mean free path λ_{a} and the transmission factor K. These last two parameters may be energy-dependent: $\lambda_{\mathrm{a}} = \lambda_{\mathrm{a}}(E)$ and $K = K(E)$.

Numerous BEES results demonstrate that the variations of I_{BEEM} in terms of bias voltage may be assumed to be linear about 0.2 V above the threshold value V_{SB}. For high voltages (above ≈ 1.8 V), the ballistic current saturates mainly because of the quantum transmission factor whose value reaches a maximum [10] and inelastic mean free path which decreases as a function of electron energy. For Au/n-Si contacts, this gives an energy window ranging from 1 to 1.8 eV in which I_{BEEM} is proportional to the electron energy. The following expression for K is therefore used:

$$K = T(V_{\mathrm{t}} - V_{\mathrm{SB}}). \quad (2)$$

This total transmission factor K only depends on the local Schottky barrier height V_{SB}, bias voltage V_{t} and interface transmission factor T.

BEEM imaging may be used to determine the electron mean free path λ_{a} because different current values can be obtained at each point of a large area. Indeed, BEEM images show contrasts that may differ from one place to another and form well-defined domains. On the other hand, spectroscopy may reveal the transport properties only for a precise tip location on the metal surface.

Two methods have been used. In the first method, the collector current is averaged over a large scale BEEM image using a constant bias voltage. This current is then divided by the tunneling current used (generally in the 1–20 nA range) yielding the following relationship:

$$I_{\mathrm{M}} = \frac{\overline{I_{\mathrm{BEEM}}}}{I_{\mathrm{tunnel}}}.$$

It should be noted that the results are independent of the tunneling current value. This experiment has been reproduced with different metal thicknesses and the same bias voltage. A d-dependent curve $\ln(I_{\mathrm{M}})$ is then obtained whose slope gives $1/\lambda_{\mathrm{a}}$ and origin ordinate the K factor.

The second method relies on variations of I_{M} in terms of bias voltage V_{t} in the 1 to 1.8 V range in increments of 0.1 V. The slope of curve I_{M} as a function of V_{t} is $s = \bar{T}\mathrm{e}^{-d/\lambda_{\mathrm{a}}}$ where $\bar{T}$ is the transmission factor for zero thickness. A logarithmic graph of this slope with respect to d, allows λ_{a} and $\bar{T}$ to be calculated. A slight modification consists in using the histogram of the BEEM current values of each image rather than the data average. As a result the most probable current value can be included in the computations. These two methods are very much alike and have been used for comparison purposes.

4 Results

To obtain a broad distribution of collector currents, large scale images have been used as shown in Figure 2. Scan size and metal thickness are 160 × 160 nm^2 and 12 nm, respectively. STM topography shows the well-known granular structure of the non-epitaxial gold layer. The two large bumps in the lower right and upper left corners give very low currents. On the other hand, the central part reveals large variations in BEEM current with domains following grain boundaries. It should be noted that during the

Table 1. Quantum transmission factors and electron mean free paths as a function of electron energy calculated using the first method.

V_t (V)	1	1.1	1.2	1.3	1.4	1.5	1.6	1.7	1.8
$T \times 1000$ (V^{-1})	4.29	5.96	6.746	6.248	8.338	7.742	7.002	7.661	7.469
λ_a (nm)	11	9.4	9.8	11.4	9	10.4	11.3	10.1	10.4

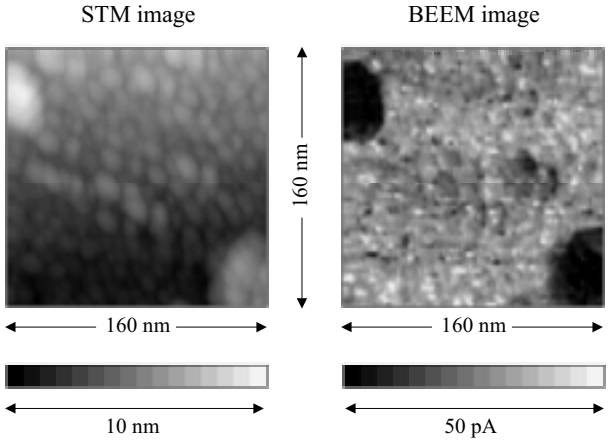

Fig. 2. STM topography (left) and BEEM image (right) of a 12 nm-thick gold layer deposited on Si(100) observed at a bias voltage of 1.8 V and a tunneling current of 5 nA. Scan size is 160 × 160 nm^2. Maximum corrugation of the gold surface is 10 nm for maximum collector current variations of about 50 pA (low current areas are depicted by dark grey levels).

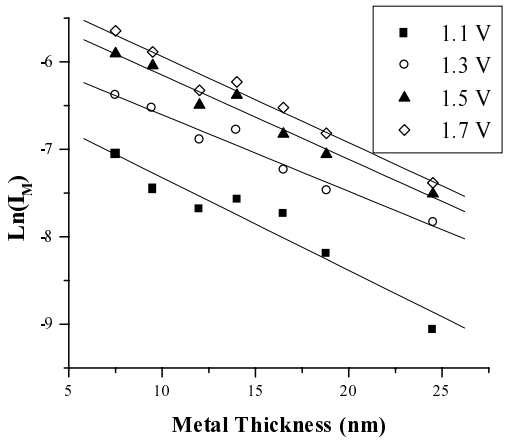

Fig. 3. Logarithm of $I_M = I_{BEEM}/I_{tunnel}$ as a function of metal thickness for four different bias voltages: 1.1, 1.3, 1.5 and 1.7 V. Each line stands for the linear fit computed using the least mean squares method.

various acquisitions (*i.e.*, with a different bias voltage), the tip has to scan the same place on the sample surface in spite of thermal drift.

First method

Figure 3 gives the I_M logarithm as a function of metal thickness limited to four different bias voltages (1.1, 1.3, 1.5 and 1.7 V) for clarity. As expected, I_M exponentially depends on the metal thickness and the logarithm is linear. The results for the nine bias voltages are listed in Table 1.

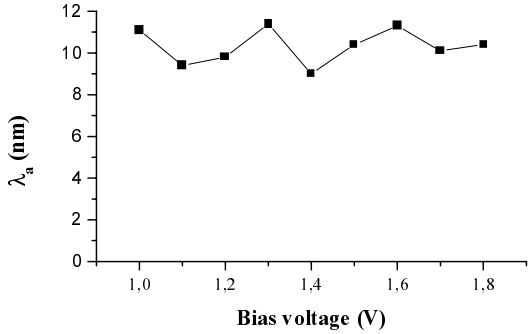

Fig. 4. Electron mean free path as a function of bias voltage. In this energy range, no dependence as a function of energy can be evidenced. A mean value of 10.3 nm has been computed.

It is shown that the electron mean free path seems independent of the injection energy between 1 and 1.8 eV as shown in Figure 4. The average value is 10.3 nm and the maximum variations of λ_a are below 20% in this energy window. The T factor also given in Table 1 has been computed using a Schottky barrier height of 0.78 eV which is the most probable threshold found using ballistic electron emission spectroscopy [11]. A slight variation in T can be shown as a function of energy.

Second method

In the second method, a set of BEEM images from the same sample but at different bias voltages is used. Figure 5a shows the results obtained for the seven thicknesses. In fact, each curve corresponds to the "average spectrum" that might be obtained on each sample. As expected, the variation is linear and the slopes "s" can be easily computed (their values being given on each curve). In Figure 5b, the logarithm of s is given in terms of thickness d. The variation $s(d)$ is found to be exponential and a value $\lambda_a = 10.7$ nm has been calculated. The origin ordinate value yields the mean transmission factor for zero thickness: $\bar{T} = 8.36 \times 10^{-3}$ V^{-1}. It should be noted that each point represented in Figures 3 and 5a has been calculated using three sets of experiments with different tips and sample locations. Note also that the model allows the different results to be fitted with a good accuracy despite the large discrepancies of current values.

On the other hand, these discrepancies may be overcome by computing the weighted average of the BEEM current over the entire image. This can easily be done using the histogram of each image whose maximum gives

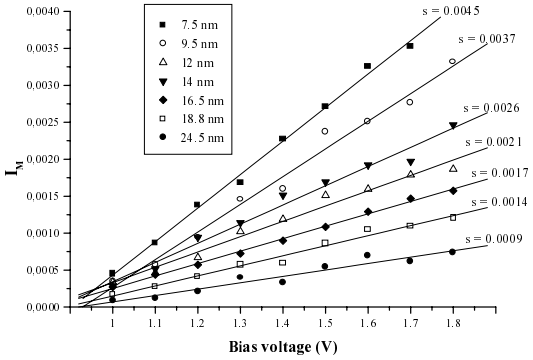

(a)

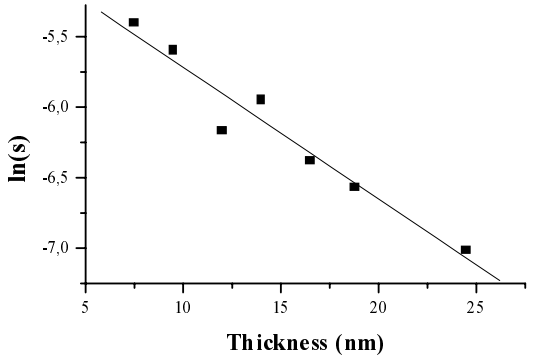

(b)

Fig. 5. (a) Variations of $I_{\mathrm{M}} = I_{\mathrm{BEEM}}/I_{\mathrm{tunnel}}$ as a function of bias voltage for seven different samples. Thickness ranges from 7.5 nm to 24.5 nm. The slope of each curve "s" derived from a linear fit is also given for each thickness. (b) Logarithm of the slope "s" as a function of thickness as derived from Figure 4a. An electron mean free path of 10.7 nm may be obtained from the linear fit.

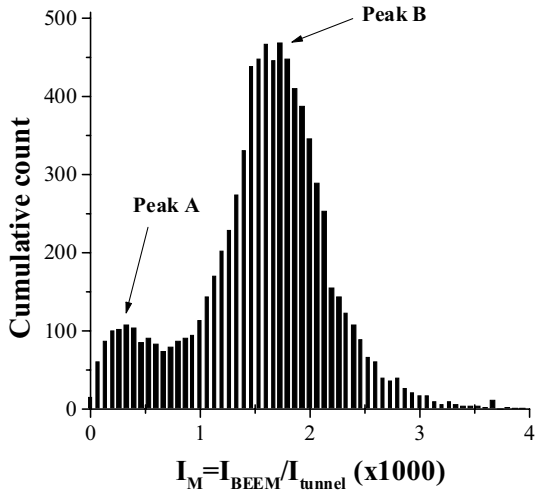

Fig. 6. Histogram of a BEEM image showing two typical peaks referred to as A (low intensity) and B (high intensity) respectively. Sample thickness and bias voltage are 16.5 nm and 1.8 V, respectively. The relative intensity of each peak depends on the low and high BEEM current area.

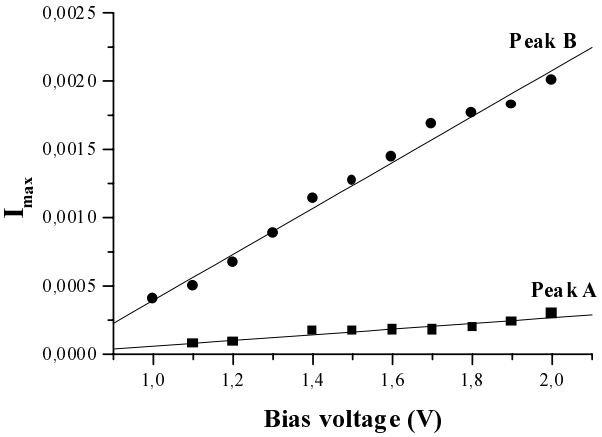

Fig. 7. Variations of peak positions as a function of bias voltage. Sample thickness is 18.8 nm. The different parameters derived from this curve are given in Table 2.

the most probable current value and prevents sharp variations in collector signal from being taken into account. This method has been applied to samples of 9.5, 12, 16.5 and 24.5 nm. Using the calculations of the 2nd method, values of $\lambda_{\mathrm{a}} = 10.9$ nm and $\bar{T} = 8.63 \times 10^{-3}$ V^{-1} have been determined.

Small scale images

As already pointed out, large scale images allow a great number of different injection yields to be taken into account. However, the mean value retained in the different methods may hide interesting local properties. Then, small scale images (typically 40 × 40 nm^2) were studied. Usually, these images feature a limited number of domains and collector currents varying greatly according to the domain considered (as shown in the centre of Fig. 5 in [11]). In this case, the histograms of these images may present two characteristic peaks whose relative intensity depends on areas of low and high ballistic current on the BEEM image. An example of this is given in Figure 6. Using the derivative of the second method, each peak may be independently studied. The curve shown in Figure 7 is derived from these computations for an 18.8 nm gold thickness. It depicts the evolution of the peak position (always a value given by $I_{\mathrm{BEEM}}/I_{\mathrm{tunnel}}$) in terms of tip-sample bias voltage. Low and high intensity peaks are called A and B, respectively. It is demonstrated that the peak position linearly depends on the electron energy, whatever the BEEM intensity observed.

These results are in good agreement with the model and equations (1, 2) could be used to determine local parameters: the slope of each curve $T\mathrm{e}^{-d/\lambda_{\mathrm{a}}}$ enables us to compute T_{A} and T_{B} (or λ_{a} for the different yields) while the origin ordinate should be proportional to V_{SB}. The results obtained for three different samples (gold thickness of 12, 16.5 and 18.8 nm) are summarized in Table 2.

It appears that the different parameters are in good agreement with our previous results. Except for the

Table 2. Local quantum transmission factors and electron mean free paths calculated from the two peaks of the BEEM images. λ_a has been computed using $T = 8.36 \times 10^{-3}$ V^{-1} while $\lambda_a = 10.9$ nm has been used for local T factors.

Gold thickness (nm)	12	16.5	18.8
Peak A: T_A (V^{-1})	1.5×10^{-3}	1.5×10^{-3}	1.12×10^{-3}
Peak A: λ_a (nm)	4.3	5.8	5
Peak A: V_{SB} (V)	0.8	0.8	0.5
Peak B: T_B (V^{-1})	8.12×10^{-3}	8.19×10^{-3}	9.55×10^{-3}
Peak B: λ_a (nm)	10.6	10.7	11.8
Peak B: V_{SB} (V)	0.78	0.83	0.76

18.8 nm sample where the peak A gives a voltage threshold of 0.5 V mainly attributed to the low BEEM intensity and to the subsequent error in the slope determination, the computed values of V_{SB} show the model to be suitable for describing electron transport from metal surface to semiconductor. T values have been computed using $\lambda_a = 10.9$ nm, those of λ_a using $T = 8.36 \times 10^{-3}$ V^{-1}.

5 Discussion

In these experiments, the ballistic current at each point of the BEEM image allows the mean current value to be obtained either through the calculated average or through image histogram. Then, the general trend of a film thickness effect may be evidenced. Although a high number of data has been used (in excess of 3×10^6), both methods clearly show that the model selected is valid. In the first method, the results demonstrate that attenuation length is independent of electron energy in the 1 to 1.8 eV range and its mean value is $\lambda_a = 10.3$ nm. Indeed, in this energy range, the dependence of the ballistic current in terms of bias voltage is generally linear [10]. The upper limit seems fairly high but neither the local BEEM spectra nor the λ_a values evidence a behaviour differing from a linear variation of I_{BEEM} in terms of V_t. Using the second method, a value of 10.9 nm has been determined with an interface transmission factor of 8.63×10^{-3} V^{-1}.

These findings are in good agreement with previous work on the measurements of λ_a in thin gold layers. In a first paper, Palm *et al.* used almost the same method to determine the attenuation length in gold for an electron energy of 1.2 eV [12] and found a value of 14 nm for λ_a. Later, Ventrice *et al.* obtained a similar value (13.3 ± 0.2 nm at room temperature and at 1.2 eV) using Ballistic Electron Emission Spectroscopy on Au/n-Si(100) contacts [13]. It should be noted that these authors report the so-called "search-light" effect which occurs when, because of the surface roughness, the electron injection angle ϑ (with respect to the surface normal) increases the electron path length to the metal/semiconductor interface as $1/\cos\vartheta$. This effect is strongly indicative of ballistic transport in the metal overlayer [14]. As a result, the collected current is reduced at large surface gradients. For a surface gradient of 60°, the BEEM current is reduced by a factor 2.5 (with λ_a =11 nm) for a metal thickness of $d = 10$ nm while this factor becomes equal to 6.2 when $d = 20$ nm. As the gold film is polycrystalline, large surface gradients are expected near grain boundaries. However, this effect has never been observed in the different experiments performed using high resolution BEEM images near grain boundaries. This can result either from a diffusive transport through the metal layer or from the tip preparation process which always produces blunt apexes unable to resolve large gradients.

Other papers which deal with the computations of electron transport, also reported the same values for λ_a (about 10 nm). Indeed, λ_a is related to the elastic λ_e and inelastic λ_i electron mean free paths through the formula $1/\lambda_a = 1/\lambda_e + 1/\lambda_i$. While λ_e mainly depends on the defect density in the metal and on phonon density in the semiconductor and is independent of energy, λ_i is governed by electron-electron interactions and has a $E^2/(E - E_F)$ dependence (where E is the electron energy above the Fermi level E_F) [15]. In their Monte-Carlo simulations, Schowalter and Lee used 10 nm and 120 nm for λ_e and λ_i respectively (*i.e.*, $\lambda_a = 9.2$ nm) for electrons 1 eV above the Fermi level [16]. Bell also used a value of 13 nm to model the room temperature spectra for a comparable gold thickness [17]. For very thin gold layers (below about 5 nm), Bell found a small increase in collector current attributed to multiple reflections within the base.

The values found in our experiments are, therefore, in good agreement with these previous investigations. One point is particularly worth emphasizing: attenuation length is not energy-dependent. From this observation, it may be concluded that transport is rather diffusive in these non-epitaxial layers. Indeed, if $\lambda_i \gg \lambda_e$, the probability of undergoing multiple elastic scattering events before inelastic scattering occurs is high. Otherwise, transport would be ballistic ($\lambda_i \approx \lambda_e$) because electrons that scatter are likely to lose one part of their kinetic energy ($\approx$ one half) and cannot overcome the potential barrier at the interface. On the other hand, a diffusive transport in which scattering is mainly due to defects and impurities in the metal overlayer is in good agreement with the non dependence of the attenuation length in terms of energy ($\lambda_a \approx \lambda_e \approx Cte$). This should downgrade resolution but measurements fail to confirm this assumption. This may be attributed to a scattering of grain boundaries inducing a confinement of the electron beam at the interface [18].

However, BEEM images present local contrasts that remain difficult to interpret. Indeed, the variations of the BEEM current observed between adjacent gold grains cannot result from thickness variations because gold grains above the average surface may present high current values (and inversely). On the other hand, we have shown that the model can be successfully applied to these local values. Then, it is assumed that the different contrasts result either from different electron mean free paths or from different transmission factors at the interface.

With respect to the first hypothesis, two different values have been computed: a one similar to those reported (about 10 nm) and a smaller one (typically 5 nm from peak A, see Tab. 2). These values may originate from the different crystallographic orientations of the gold grains with respect to the surface normal inducing electron channeling in the metal layer. As soon as the grain orientation is no longer suitable, large amounts of electrons scatter. The attenuation length is rather small and the corresponding grains exhibit very low BEEM intensities. On the other hand, λ_a may be large if the carriers are injected along a preferential direction of the scanned gold grain. Therefore, one has to assume that the local λ_a value depends of the grain crystallographic orientation. This can be observed in ionic implantation.

The different collector values may also result from the various interface transmission factors. Two values have been found: about 8×10^{-3} and 1×10^{-3} V^{-1} (other values could probably be obtained at other sample locations). This effect may be directly linked to the granular structure of the metal overlayer in which defects or contamination at the interface can dramatically alter the transmission probability. It is well-known that these defects cause grain nucleation which explains the presence of domains following the grain boundaries. This could also explain the results obtained under UHV in which the silicon surfaces are carefully prepared and the metal layer is evaporated after a well defined surstructure (*e.g.*, 7×7 for Si(111)) [19].

More recently, Garcia-Vidal *et al.* demonstrated from a theoretical perspective that the apparently identical Au/Si(100) and Au/Si(111) spectroscopic results in BEEM experiments could be attributed to an electronic structure effect in gold [20]. According to these authors, in Au(111), electrons propagate in two directions with respect to the [111] direction. The electron beams associated with these two main directions, namely [110] and [1/4 1/4 1], yield two intensities. Moreover, projection of the gold surface Brillouin zone onto the (111) plane overlaps the Brillouin zone of Silicon (100) only if the [011] direction of the metal runs parallel to the same semiconductor direction. Otherwise, the minima of the semiconductor conduction band may be located outside the electron beam directions which decreases the collector current. Therefore, one can assume that this effect occurs in the Au polycrystalline layer in which gold grains are randomly oriented with respect to the substrate normal and to the crystallographic orientations in the interface plane. The two different interface transmission factors may therefore originate from these effects on the electron beam due to the electronic and crystallographic structure of metal and semiconductor. This focusing effect in the gold layer may also account for the resolution achieved and for non-observation of the search-light effect. In this case, the electron mean free path value of 11 nm is constant and irrespective of gold grain. This interpretation does not exclude a possible role of defects at the interface which act as diffusion centres and modulate the collector current.

6 Conclusion

BEEM imaging has been used on Au/n-Si junctions to study electron transport properties in a thin metal layer. Using a model in which the collector current is assumed to decrease exponentially as a function of metal thickness, it is shown on large scale images that the electron mean free path is not energy-dependent in the 1–1.8 eV range and that transport is rather diffusive. A constant value of about 11 nm has been determined. On the other hand, using small scale images, the basic parameters (electron mean free path and/or interface transmission factor) used in the model are found to be dependent on the gold grain observed and two different yields have been evidenced. It is assumed that these observations result from the polycrystalline nature of the metal layer in which the channeling of carriers due to the overlayer crystallographic structure, electronic effects in both metal and semiconductor and defects at the interface play a major role.

The authors would like to thank M.D. Prietsch for his fruitful comments and G. Peuch for technical assistance.

References

1. L.D. Bell, W.J. Kaiser, Phys. Rev. Lett. **60**, 1406 (1988).
2. L.D. Bell, W.J. Kaiser, Phys. Rev. Lett. **61**, 2368 (1988).
3. M. Prietsch, R. Ludeke, Phys. Rev. Lett **66**, 2511 (1991).
4. A.E. Fowel, R.H. Williams, B.E. Richarson, T.H. Shen, Semicond. Sci. Technol. **5**, 348 (1990).
5. R. Coratger, F. Ajustron, J. Beauvillain, I.M. Dharmadasa, C.J. Blomfield, K.A. Prior, J. Simpson, B.C. Cavenett, Phys. Rev. B **51**, 2357 (1995).
6. B.A. Morgan, K.M. Ring, K.L. Kavanagh, A.A. Talin, R.S. Williams, T. Yasuda, T. Yasui, Y. Segawa, J. Appl. Phys. **79**, 1532 (1996) .
7. J.J. O'Shea, T. Sajoto, S. Bhargawa, D. Leonard, M.A. Chin, V. Narayanamurti, J. Vac. Sci. Technol. B **12**, 2625 (1994).
8. M. Ke, D.I. Westwood, C.C. Matthai, B. Richardson, Mat. Sci. Eng. B **35**, 349 (1995).
9. C. Eder, J. Smoliner, G. Strasser, Appl. Phys. Lett. **68**, 2876 (1996).
10. M. Prietsch, Habilitationsschrift, Freie Universitat Berlin, 1992.
11. R. Coratger, F. Ajustron, J. Beauvillain, J. Phys. III France **3**, 2211 (1993).
12. H. Palm, M. Arbes, M. Schulz, Appl. Phys. A **56**, 1 (1996).
13. C.A. Ventrice, V.P. LaBella, G. Ramaswany, H.P. Yu, L.J. Schowalter, Appl. Surf. Sci. **104**, 274 (1996).
14. A. Bauer, M.T. Cuberes, M. Prietsch, G. Kaindl, Phys. Rev. Lett. **71**, 149 (1993).
15. E.Y. Lee, H. Sirringhaus, U. Kafader, H. von Känel, Phys. Rev. B **52**, 1816 (1995).
16. L.J. Schowalter, E.Y. Lee, Phys. Rev. B **43**, 9308 (1991).
17. L.D. Bell, Phys. Rev Lett. **77**, 3893 (1996).
18. A.M. Milliken, S.J. Manion, W.J. Kaiser, L.D. Bell, M.H. Hecht, Phys. Rev. B **46**, 12826 (1992).
19. M.T. Cuberes, A. Bauer, H.J. Wen, D. Vandre, M. Prietsch, G. Kaindl, J. Vac. Sci. Technol. B **12**, 2422 (1994).
20. F.J. Garcia-Vidal, P.L. de Andres, F. Flores, Phys. Rev. Lett. **76**, 807 (1996).